Journal of Statistical and Econometric Methods, vol.6, no.1, 2017, 1-44
ISSN: 1792-6602 (print), 1792-6939 (online)
Scienpress Ltd, 2017

Simulating Uniform- and Triangular- Based Double Power Method Distributions

Mohan D. Pant[1] and Todd C. Headrick[2]

Abstract

Power method (PM) polynomials have been used for simulating non-normal distributions in a variety of settings such as toxicology research, price risk, business-cycle features, microarray analysis, computer adaptive testing, and structural equation modeling. A majority of these applications are based on the method of matching product moments (e.g., skew and kurtosis). However, estimators of skew and kurtosis can be (a) substantially biased, (b) highly dispersed, or (c) influenced by outliers. To address this limitation, two families of double-uniform-PM and double-triangular-PM distributions are characterized through the method of *L*-moments using a doubling technique. The *L*-moment based procedure is contrasted with the method of product moments in the contexts of fitting real data and estimation of parameters. A methodology for simulating correlated double-uniform-PM and double-triangular-PM distributions with specified values of *L*-skew, *L*-kurtosis, and *L*-correlation is also demonstrated. Monte Carlo simulation results indicate that the *L*-moment-based estimators of

[1]University of Texas at Arlington, Arlington, TX 76019, USA. E-mail: mpant@uta.edu
[2]Southern Illinois University Carbondale, Carbondale, IL 62901, USA.
E-mail: headrick@siu.edu

Article Info: *Received* : October 25, 2016. *Revised* : November 26, 2016.
Published online : January 25, 2017.

L-skew, L-kurtosis, and L-correlation are superior to their product moment-based counterparts.

Mathematics Subject Classification: 60E05; 62G30; 62H12; 62H20; 65C05; 65C10; 65C60; 78M05

Keywords: Product moments; Pearson correlation; L-moments; L-correlation

1 Introduction

Fleishman's [1] power method (PM) polynomial is defined as

$$p(X) = c_0 + c_1 X + c_2 X + c_3 X^3, \quad (1)$$

where X is a standard normal random variable with probability density function (pdf) and cumulative distribution function (cdf) given respectively as $\phi(x) = \left(\sqrt{2\pi}\right)^{-1} e^{-x^2/2}$ and $\Phi(x) = \int_{-\infty}^{x} \phi(x)dx$. Headrick [2] has extended the third-order PM to fifth-order PM polynomial transformation for generating univariate and multivariate non-normal distributions (see also [3]).

The PM polynomial in (1) has been widely used in a variety of applied mathematics fields (especially, in the contexts of statistical modeling and simulation). Some of the examples of such applications are: Asset pricing theory [4], multivariate analysis [5], business-cycle features [6], microarray analysis [7], price risk [8], analysis of covariance (ANCOVA) [9, 10], analysis of variance (ANOVA) [11-13], regression analysis [14], nonparametric statistics [15], item response theory [16], toxicology research [17], structural equation modeling [18], correlation studies [19], Monte Carlo simulation studies [20, 21], and L-moment-based characterizations [22-24].

The logistic-, uniform-, and triangular- based PM polynomials have been developed and studied by Hodis and Headrick [25] and Hodis [26] with the purpose of extending the range of possible values of skew and kurtosis associated

with a non-normal distribution (see also [23]). In order to produce a valid non-normal distribution, the PM polynomial in (1) has to be a strictly increasing monotone function. This requirement implies that an inverse function (p^{-1}) exists. As such, the parametric forms of cdf and pdf associated with (1) can be expressed as [3] (see also [27])

$$F\big(p(x)\big) = F\big(p(x), \Phi(x)\big) \tag{2}$$

$$f\big(p(x)\big) = f\big(p(x), \phi(x)/p'(x)\big) \tag{3}$$

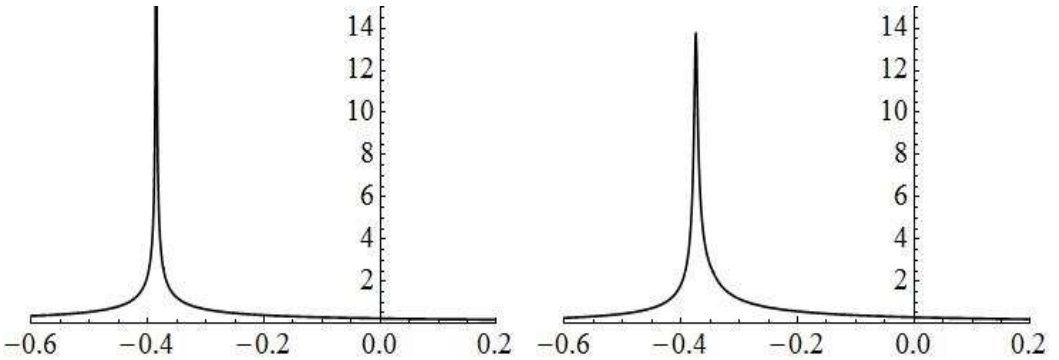

$c_0 = -0.372054, c_1 = 0.164150,$ $c_2 = 0.710570,$ and $c_3 = 1.119402$

A

$c_0 = -0.344536, c_1 = 0.164747,$ $c_2 = 0.329008,$ and $c_3 = 0.256520$

B

Figure 1: The pdfs of uniform-based third-order PM distribution with skew = 1.3 and kurtosis = 1.25 (Panel A) and triangular-based third-order PM distribution with skew = 2.3 and kurtosis = 6.9 (Panel B). The values of coefficients $c_{i=0,1,2,3}$ for the two pdfs (Panels A and B) were determined by solving the systems of equations (13)—(16) from Hodis et al. ([23], p. 2164) after replacing the associated moments from corresponding $Unif(-\sqrt{\pi/2}, \sqrt{\pi/2})$ and $Tri(-\sqrt{2\pi}, \sqrt{2\pi})$ distributions.

One of the limitations associated with the product-moment based PM polynomials is that the non-normal distributions with values of skew and (or) kurtosis that lie in the upper right region of the skew-kurtosis boundary graph (e.g., [23, pages 2165-2168]) can be excessively leptokurtic and therefore may not be representative of real world data. To illustrate this limitation in the context of this study, Figure 1 shows pdfs of uniform-based PM polynomial with skew (γ_3) of 1.3 and kurtosis (γ_4) of 1.25 (Panel A) and triangular-based PM polynomial with skew (γ_3) of 2.3 and kurtosis (γ_4) of 6.9 (Panel B). Figure 1 (Panels A and B) illustrates the excessive leptokurtic behavior of some of the uniform- and triangular-based PM distributions.

In order to obviate the above limitation, the main purpose of this study is to characterize two families of uniform- and triangular-based double PM distributions using a doubling technique introduced by Morgenthaler and Tukey [28]. Specifically, the two families of double-uniform-PM and double-triangular-PM distributions can be derived using special cases of PM polynomials in (1) and a doubling technique [24, 28] as:

$$p(U) = \begin{cases} U + C_{\mathcal{L}}\, U^3, & \text{for } U \leq 0 \\ U + C_{\mathcal{R}}\, U^3, & \text{for } U \geq 0 \end{cases} \tag{4}$$

$$p(T) = \begin{cases} T + C_{\mathcal{L}}\, T^3, & \text{for } T \leq 0 \\ T + C_{\mathcal{R}}\, T^3, & \text{for } T \geq 0 \end{cases} \tag{5}$$

where the random variables U and T in (4) and (5) are drawn from symmetric uniform $U \sim Unif(-\sqrt{\pi/2}, \sqrt{\pi/2})$ and triangular $T \sim Tri(-\sqrt{2\pi}, \sqrt{2\pi})$ distributions, respectively. These specific forms of uniform and triangular distributions are used so that the maximum height of pdfs associated with the double-uniform-PM and double-triangular-PM distributions in (4) and (5) is equal to the maximum height $\left(1/\sqrt{2\pi}\right)$ of standard normal pdf.

To demonstrate, given in Figure 2 are the pdfs of double-uniform-PM with skew (γ_3) of 1.3 and kurtosis (γ_4) of 1.25 (Panel A) and double-triangular-PM

with γ_3 of 2.3 and γ_4 of 6.9 (Panel B). Inspection of Fig. 2 (Panels A and B) indicates that the double-uniform-PM and double-triangular-PM distributions are less leptokurtic and more suitable for fitting real-world data compared to the traditional third-order PM distributions in Figure 1 (Panels A and B). Note that the values of γ_3 and γ_4 for the two distributions in Figure 2 (Panels A and B) are equal to those associated with the two distributions in Figure 1 (Panels A and B). The solved values of $C_{\mathcal{L}}$ and $C_{\mathcal{R}}$ for the two distributions in Figure 2 are obtained by solving systems of equations (9)—(10) and (14)—(15), respectively.

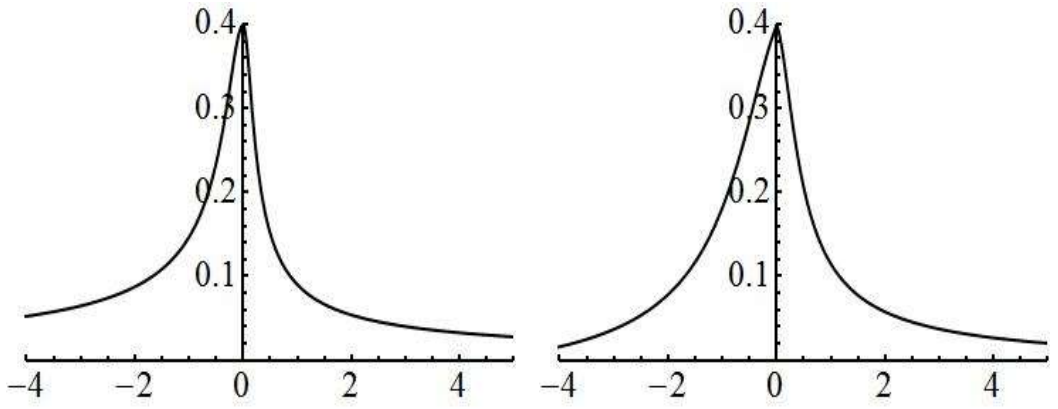

$C_{\mathcal{L}} = 1.419686,\ C_{\mathcal{R}} = 5.267159$ $C_{\mathcal{L}} = 0.187949,\ C_{\mathcal{R}} = 1.216440$

A B

Figure 2: The pdfs of double-uniform-PM distribution with skew = 1.3 and kurtosis = 1.25 (Panel A) and double-triangular-PM distribution with skew = 2.3 and kurtosis = 6.9 (Panel B). The values of coefficients $C_{\mathcal{L}}$ and $C_{\mathcal{R}}$ for the two pdfs (Panels A and B) were determined by solving the systems of equations (9)—(10) and (14)—(15), respectively. Note that the values of skew and kurtosis for these two distributions are equal to those associated with two distributions in Figure 1 (Panels A and B).

The product moment-based PM polynomials have their own disadvantages insofar as the estimates of skew and kurtosis associated with non-normal

distributions can be (a) substantially biased, (b) highly dispersed, or (c) influenced by outliers [22-24, 29-32], and thus may not be good representatives of the true parameters. To illustrate this limitation, provided in Table 1 are the values of parameters and sample estimates of skew (γ_3) and kurtosis (γ_4) for the distributions in Fig. 2 (Panels A and B). Inspection of Table 1 indicates that the bootstrap estimates ($\hat{\gamma}_3$ and $\hat{\gamma}_4$) of skew (γ_3) and kurtosis (γ_4) are substantially attenuated below and above their corresponding parameter values. Additionally, there is greater bias and dispersion in the estimates associated with distribution with greater departure from normality. Specifically, for the distribution in Fig. 2B (for the sample size $n = 25$), the estimates ($\hat{\gamma}_3$ and $\hat{\gamma}_4$) are 76.83%, and 66.39% of their corresponding parameters (γ_3 and γ_4), respectively. The estimates ($\hat{\gamma}_3$ and $\hat{\gamma}_4$) of skew and kurtosis (γ_3 and γ_4) in Table 1 were calculated based on Fisher's k-statistics formulae from Kendall and Stuart [33, pages 299-300], currently used by most commercial software packages such as SAS, SPSS, Minitab, etc., for computing the values of skew and kurtosis (where $\gamma_{3,4} = 0$ for the standard normal distribution).

Table 1: Product moment-based parameters (γ_3, γ_4) of skew and kurtosis and their bootstrap estimates $(\hat{\gamma}_3, \hat{\gamma}_4)$ for the pdfs in Figure 2A and Figure 2B. Each bootstrap estimate, associated 95% confidence interval (95% C.I.), and the standard error (SE) were based on resampling 25000 statistics. Each statistic was based on a sample size of $n = 25$.

Distribution	Parameter	Estimate	95% C.I.	SE	RSE%
Fig. 2A	$\gamma_3 = 1.3$	$\hat{\gamma}_3 = 1.276$	(1.2699, 1.2817)	0.0030	0.2351
	$\gamma_4 = 1.25$	$\hat{\gamma}_4 = 1.699$	(1.6743, 1.7242)	0.0128	0.7534
Fig. 2B	$\gamma_3 = 2.3$	$\hat{\gamma}_3 = 1.767$	(1.7565, 1.7779)	0.0055	0.3113
	$\gamma_4 = 6.9$	$\hat{\gamma}_4 = 4.581$	(4.5345, 4.6279)	0.0240	0.5239

Note. RSE% = 100×(SE/Estimate).

In order to address above limitations, Pant and Headrick [24] have characterized double-normal-PM and double-logistic-PM distributions through L-moment-based procedure and contrasted it with the product moment-based procedure. Additionally, to address the latter limitation, Headrick [22] has characterized the third- and fifth-order PM distributions through the method of L-moments. The method of L-moments introduced by Hosking [29] is an attractive alternative to product moment-based method as it can be used in fitting theoretical and empirical distributions, estimating parameters, and testing of hypothesis [29-31]. In the context of non-normal distributions, some of the advantages that L-moment based estimators have over product moments are that they (a) exist whenever the mean of the distribution exists, (b) are nearly unbiased for all sample sizes and distributions, and (c) are more robust in the presence of outliers [29-31, 22, 34].

Table 2: L-moment based parameters (τ_3, τ_4) of L-skew and L-kurtosis and their bootstrap estimates $(\hat{\tau}_3, \hat{\tau}_4)$ for the pdfs in Figure 2A and Figure 2B. Each bootstrap estimate, associated 95% confidence interval (95% C.I.), and the standard error (SE) were based on resampling 25000 statistics. Each statistic was based on a sample size of $n = 25$.

Distribution	Parameter	Estimate	95% C.I.		SE	RSE%
Fig. 2A	$\tau_3 = 0.2730$	$\hat{\tau}_3 = 0.2702$	(0.2661,	0.2712)	0.0005	0.1850
	$\tau_4 = 0.2169$	$\hat{\tau}_4 = 0.2292$	(0.2280,	0.2304)	0.0006	0.2618
Fig. 2B	$\tau_3 = 0.3334$	$\hat{\tau}_3 = 0.3127$	(0.3111,	0.3145)	0.0009	0.2878
	$\tau_4 = 0.3249$	$\hat{\tau}_4 = 0.3254$	(0.3241,	0.3266)	0.0006	0.1844

Note. RSE% = 100×(SE/Estimate).

For example, provided in Table 2 are the bootstrap estimates ($\hat{\tau}_3$ and $\hat{\tau}_4$) of L-moment-based parameters of L-skew and L-kurtosis (τ_3 and τ_4) along with their corresponding 95% confidence intervals associated with the double-uniform-PM and double-triangular-PM distributions in Fig. 2 (Panels A

and B). The L-moment-based estimates ($\hat{\tau}_3$ and $\hat{\tau}_4$) of L-skew and L-kurtosis (τ_3 and τ_4) in Table 2 are relatively closer to their respective parameter values with much smaller variance compared to their product moment-based counterparts. Inspection of Table 2 shows that for the distribution in Figure 2B (for the sample size $n = 25$), the values of the estimates are on average 93.79% and 100.15% of their corresponding parameters.

The remainder of the paper is organized as follows. In Section 2, the systems of equations for the product moment-based skew (γ_3) and kurtosis (γ_4) associated with the two families of double-uniform-PM and double-triangular-PM distributions are derived. Also provided in Section 2 is a methodology for solving the systems of equations for the shape parameters ($C_{\mathcal{L}}$ and $C_{\mathcal{R}}$) associated with these families of distributions. In Section 3, a brief introduction to L-moments is given. Section 3 also provides the derivation of the systems of equations for the L-moment-based L-skew (τ_3) and L-kurtosis (τ_4) for the two families. Also provided in Section 3 is an L-moment-based methodology for solving the systems of equations for the shape parameters ($C_{\mathcal{L}}$ and $C_{\mathcal{R}}$) associated with the two families. In Section 4, a comparison between product moment- and L-moment-based double-uniform-PM and double-triangular-PM distributions is presented in the context of fitting real-world data and estimation of parameters. In Section 5, a methodology for simulating multivariate distributions with specified L-correlation structure is described. Provided in Section 6 is an example to demonstrate the multivariate data generation. In Section 7, the simulation results are provided and discussed.

2 Product Moment-Based Methodology

2.1 Product Moment-Based Double-Uniform-PM Distributions

The product moments $\left(\mu_{r=1,\dots,4}\right)$ associated with (4) can be obtained from

$$\mu_r = \int_{-\sqrt{\pi/2}}^{0} (u + C_{\mathcal{L}} u^3)^r \, \phi(u) du + \int_{0}^{\sqrt{\pi/2}} (u + C_{\mathcal{R}} u^3)^r \, \phi(u) du. \tag{6}$$

where $\phi(u) = 1/\sqrt{2\pi}$ is the pdf of $Unif(-\sqrt{\pi/2}, \sqrt{\pi/2})$ distribution.

The mean (μ), variance (σ^2), skew (γ_3), and kurtosis (γ_4) of double-uniform-PM distributions can be given using formulae in [33] as:

$$\mu = \frac{(C_{\mathcal{R}} - C_{\mathcal{L}})\pi^{3/2}}{16\sqrt{2}} \tag{7}$$

$$\sigma^2 = \frac{\pi}{6} + \frac{1}{20}(C_{\mathcal{L}} + C_{\mathcal{R}})\pi^2 + \frac{\left(25{C_{\mathcal{L}}}^2 + 14C_{\mathcal{L}}C_{\mathcal{R}} + 25{C_{\mathcal{R}}}^2\right)\pi^3}{3584} \tag{8}$$

$$\begin{aligned}\gamma_3 = -[6\sqrt{105}(C_{\mathcal{L}} - C_{\mathcal{R}})\pi\Big(4480 + 9\pi\Big(224(\mathrm{C}_{\mathcal{L}} + \mathrm{C}_{\mathcal{R}}) + 3\pi(9\mathrm{C}_{\mathcal{L}}^2 + \\ + 14\mathrm{C}_{\mathcal{L}}\mathrm{C}_{\mathcal{R}} + 9\mathrm{C}_{\mathcal{R}}^2)\Big)\Big)]/[8960 + 3\pi\Big(896(\mathrm{C}_{\mathcal{L}} + \mathrm{C}_{\mathcal{R}}) + 5\pi(25\mathrm{C}_{\mathcal{L}}^2 + \\ + 14\mathrm{C}_{\mathcal{L}}\mathrm{C}_{\mathcal{R}} + 25\mathrm{C}_{\mathcal{R}}^2)\Big)]^{3/2}\end{aligned} \tag{9}$$

$$\begin{aligned}\gamma_4 = \big[6\{&-2296053760 - 984023040(C_{\mathcal{L}} + C_{\mathcal{R}})\pi \\ &+ 512512\left(67{C_{\mathcal{L}}}^2 - 966C_{\mathcal{L}}C_{\mathcal{R}} + 67{C_{\mathcal{R}}}^2\right)\pi^2 \\ &+ 174720(C_{\mathcal{L}} + C_{\mathcal{R}})\left(491{C_{\mathcal{L}}}^2 - 854C_{\mathcal{L}}C_{\mathcal{R}} + 491{C_{\mathcal{R}}}^2\right)\pi^3 \\ &+ 165\left(65773{C_{\mathcal{L}}}^4 + 26572{C_{\mathcal{L}}}^3C_{\mathcal{R}} - 82290{C_{\mathcal{L}}}^2{C_{\mathcal{R}}}^2\right. \\ &\left.+ 26572C_{\mathcal{L}}{C_{\mathcal{R}}}^3 + 65773{C_{\mathcal{R}}}^4\right)\pi^4\}\big] \\ &/\big[143(8960 + 3\pi(896(C_{\mathcal{L}} + C_{\mathcal{R}}) + 5\pi(25{C_{\mathcal{L}}}^2 + 14C_{\mathcal{L}}C_{\mathcal{R}} \\ &+ 25{C_{\mathcal{R}}}^2)))^2\big]\end{aligned} \tag{10}$$

2.2 Product Moment-Based Double-Triangular-PM Distributions

The product moments $\left(\mu_{r=1,\ldots,4}\right)$ associated with (5) can be obtained from

$$\mu_r = \int_{-\sqrt{2\pi}}^{0} (t + C_{\mathcal{L}} t^3)^r \, \phi(t) dt + \int_{0}^{\sqrt{2\pi}} (t + C_{\mathcal{R}} t^3)^r \, \phi(t) dt. \tag{11}$$

where $\phi(t) = \begin{cases} \left(\sqrt{2\pi} + t\right)/2\pi\,, & \text{for } t \leq 0 \\ \left(\sqrt{2\pi} - t\right)/2\pi\,, & \text{for } t > 0 \end{cases}$ is the pdf of $Tri(-\sqrt{2\pi}, \sqrt{2\pi})$ distribution.

The mean (μ), variance (σ^2), skew (γ_3), and kurtosis (γ_4) of double-triangular-PM distributions can be given using formulae in [33] as:

$$\mu = \frac{(C_{\mathcal{R}} - C_{\mathcal{L}})\pi^{3/2}}{5\sqrt{2}} \tag{12}$$

$$\sigma^2 = \frac{\pi(350 + 280\pi(C_{\mathcal{L}} + C_{\mathcal{R}}) + 3\pi^2(43{C_{\mathcal{L}}}^2 + 14C_{\mathcal{L}}C_{\mathcal{R}} + 43{C_{\mathcal{R}}}^2))}{1050} \tag{13}$$

$$\begin{aligned} \gamma_3 = -[2\sqrt{21}(C_{\mathcal{L}} - C_{\mathcal{R}})\pi \Big(& 10725 \\ & + 2\pi \Big(7315(C_{\mathcal{L}} + C_{\mathcal{R}}) \\ & + 81\pi\left(38{C_{\mathcal{L}}}^2 + 49C_{\mathcal{L}}\,C_{\mathcal{R}} + 38{C_{\mathcal{R}}}^2\right)\Big)\Big)] \\ & /[11\{\Big(350 + 280\pi(C_{\mathcal{L}} + C_{\mathcal{R}}) \\ & + 3\pi^2\left(43{C_{\mathcal{L}}}^2 + 14C_{\mathcal{L}}\,C_{\mathcal{R}} + 43{C_{\mathcal{R}}}^2\right)\Big)\}^{3/2}] \end{aligned} \tag{14}$$

$$\begin{aligned} \gamma_4 = \big[6\{ & -1751750 + 1001000\pi(C_{\mathcal{L}} + C_{\mathcal{R}}) + 200200\pi^2(55{C_{\mathcal{L}}}^2 \\ & - 17C_{\mathcal{L}}C_{\mathcal{R}} + 55{C_{\mathcal{R}}}^2) + 3640\pi^3(C_{\mathcal{L}} + C_{\mathcal{R}})(3887{C_{\mathcal{L}}}^2 \\ & - 4074C_{\mathcal{L}}C_{\mathcal{R}} + 3887{C_{\mathcal{R}}}^2) + 3\pi^4(1803829{C_{\mathcal{L}}}^4 \\ & + 502684{C_{\mathcal{L}}}^3C_{\mathcal{R}} - 598026{C_{\mathcal{L}}}^2{C_{\mathcal{R}}}^2 + 502684C_{\mathcal{L}}{C_{\mathcal{R}}}^3 \\ & + 1803829{C_{\mathcal{R}}}^4)\}\big] \\ & /\big[143(350 + 280\pi(C_{\mathcal{L}} + C_{\mathcal{R}}) + 3\pi^2(43{C_{\mathcal{L}}}^2 + 14C_{\mathcal{L}}C_{\mathcal{R}} \\ & + 43{C_{\mathcal{R}}}^2))^2\big] \end{aligned} \tag{15}$$

The product-moment-based procedure for simulating the double-uniform-PM and double-triangular-PM distributions involves a moment-matching approach in

which specified values of skew (γ_3) and kurtosis (γ_4) are substituted on the left-hand sides of (9)—(10) and (14)—(15), respectively, and then these systems are simultaneously solved for the shape parameters ($C_{\mathcal{L}}$ and $C_{\mathcal{R}}$). The solved values of $C_{\mathcal{L}}$ and $C_{\mathcal{R}}$ can be substituted into (7)—(8) and (12)—(13), respectively, to determine the values of mean and variance associated with the double-uniform-PM and double-triangular-PM distributions. The solved values of $C_{\mathcal{L}}$ and $C_{\mathcal{R}}$ can be substituted into (4) and (5) to generate the double-uniform-PM and double-triangular-PM distributions, respectively, with specified values of skew and kurtosis. Eventually, (4) and (5) can be substituted into (3) to obtain the parametric plots of the pdfs associated with the corresponding distributions. For example, the pdfs of double-uniform-PM and double-triangular-PM distributions in Figure 2 (Panels A and B) were plotted by first substituting the solved values of (A) $C_{\mathcal{L}} = 1.419686$ and $C_{\mathcal{R}} = 5.267159$ into (4) and (B) $C_{\mathcal{L}} = 0.187949$ and $C_{\mathcal{R}} = 1.216440$ into (5), respectively, for generating the double-uniform-PM and the double-triangular-PM distributions, and substituting them separately into (3) for the parametric forms of corresponding pdfs.

The boundary graphs plotted in $|\gamma_3| - \gamma_4$ plane in Figure 3 (Panel A and Panel B) can be used for finding possible combinations of skew (γ_3) and kurtosis (γ_4) associated with product moment-based double-uniform-PM and double-triangular-PM distributions. Figure 3 (Panel A) shows the boundary graph for possible combinations of skew (γ_3) and kurtosis (γ_4) associated with a valid double-uniform-PM distribution, where the values of $|\gamma_3|$ range between 0 and 2.0573 and those of γ_4 range between -1.2 to 3.2381. Figure 3 (Panel B) shows the boundary graph for possible combinations of skew (γ_3) and kurtosis (γ_4) associated with a valid double-triangular-PM distribution, where the values of $|\gamma_3|$ range between 0 and 3.5007 and those of γ_4 range between -0.6 to 13.6443.

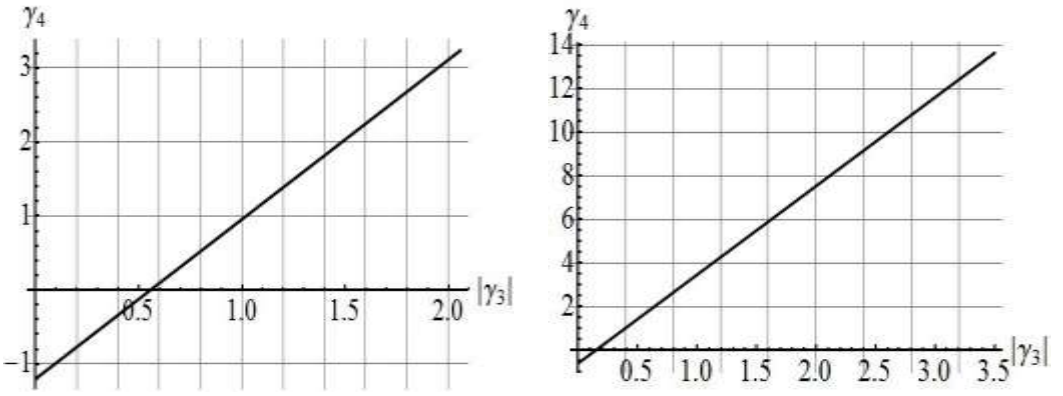

A B

Figure 3: Boundary graphs of the regions for possible combinations of (absolute value) skew ($|\gamma_3|$) and kurtosis (γ_4) for the symmetric double-uniform-PM (Panel A) and double-triangular-PM (Panel B) distributions.

3 *L*-Moment-Based Methodology

3.1 Preliminaries for *L*-Moments

Let $Y_1, Y_2, \dots, Y_i, \dots, Y_n$ be independently and identically distributed random variables each with pdf $f(y)$, cdf $F(y)$, then the first four L-moments are defined as [31, pages 20-22]:

$$\lambda_1 = \beta_0 \tag{16}$$

$$\lambda_2 = 2\beta_1 - \beta_0 \tag{17}$$

$$\lambda_3 = 6\beta_2 - 6\beta_1 + \beta_0 \tag{18}$$

$$\lambda_4 = 20\beta_3 - 30\beta_2 + 12\beta_1 - \beta_0 \tag{19}$$

where coefficients associated with $\beta_{r=0,1,2,3}$ in (16)—(19) are derived from shifted orthogonal Legendre polynomials and are computed as described in [31, page 20] and where β_r is the rth weighted probability moment (PWM) defined as:

$$\beta_r = \int y\{F(y)\}^r f(y)dy \tag{20}$$

The L-moments λ_1 and λ_2 in (16)—(17) are measures of location and scale parameters and are equal to the arithmetic mean and one-half of the coefficient of mean difference or Gini's index [33, pages 47-48]. In the literature of L-moments (e.g., [29]), the dimensionless ratios of higher order L-moments (i.e., λ_3 and λ_4) to λ_2 are referred to as L-skew (τ_3) and L-kurtosis (τ_4), respectively. Thus, the formulae for L-skew (τ_3) and L-kurtosis (τ_4) are given as:

$$\tau_3 = \frac{\lambda_3}{\lambda_2} \tag{21}$$

$$\tau_4 = \frac{\lambda_4}{\lambda_2} \tag{22}$$

In general, the indices of L-skew (τ_3) and L-kurtosis (τ_4) are bounded such that $|\tau_3| < 1$ and $|\tau_4| < 1$, and a symmetric distribution has L-skew $(\tau_3) = 0$ [22].

Estimates of L-moments from a sample (n) of real data can be computed as a linear combination of the sample order statistics $Y_{1:n} \leq Y_{2:n} \leq \cdots \leq Y_{n:n}$. The unbiased sample estimates of the PWMs are given as [29]:

$$\hat{\beta}_r = \frac{1}{n}\sum_{i=r+1}^{n} \frac{(i-1)(i-2)\ldots(i-r)}{(n-1)(n-2)\ldots(n-r)} Y_{i:n} \tag{23}$$

where $r = 0, 1, 2, 3$. Here, $\hat{\beta}_0$ is the sample mean. The first four sample L-moments $(\hat{\lambda}_1, \hat{\lambda}_2, \hat{\lambda}_3, \hat{\lambda}_4)$ are obtained by substituting $\hat{\beta}_r$ instead of β_r in equations (16)−(19). The sample estimates of L-skew and L-kurtosis are denoted as $\hat{\tau}_3$ and $\hat{\tau}_4$, where $\hat{\tau}_3 = \hat{\lambda}_3/\hat{\lambda}_2$ and $\hat{\tau}_4 = \hat{\lambda}_4/\hat{\lambda}_2$.

3.2 *L*-Moment-Based Double-Uniform-PM Distributions

The L-moment-based system of equations for the double-uniform-PM distributions can be derived by first defining the PWMs based on (20) in terms of

$p(U)$ in (4) and the uniform pdf $\phi(u) = 1/\sqrt{2\pi}$ and cdf $\Phi(u) = \left(u + \sqrt{\pi/2}\right)/\sqrt{2\pi}$ as

$$\beta_r = \int_{-\sqrt{\pi/2}}^{0} (u + C_{\mathcal{L}}\, u^3)\{\Phi(u)\}^r \phi(u) du + \int_{0}^{\sqrt{\pi/2}} (u + C_{\mathcal{R}}\, u^3)\{\Phi(u)\}^r \phi(u) du. \tag{24}$$

Integrating (24) for $\beta_{r=0,1,2,3}$ and substituting into (16)—(19) yields the first four L-moments; which are eventually substituted into (21)—(22) to obtain the following system of equations:

$$\lambda_1 = \frac{(C_{\mathcal{R}} - C_{\mathcal{L}})\pi^{3/2}}{16\sqrt{2}} \tag{25}$$

$$\lambda_2 = \frac{\sqrt{\pi}\left(20 + 3\pi(C_{\mathcal{L}} + C_{\mathcal{R}})\right)}{60\sqrt{2}} \tag{26}$$

$$\tau_3 = \frac{15(C_{\mathcal{R}} - C_{\mathcal{L}})\pi}{24(C_{\mathcal{L}} + C_{\mathcal{R}})\pi + 160} \tag{27}$$

$$\tau_4 = \frac{6(C_{\mathcal{L}} + C_{\mathcal{R}})\pi}{21(C_{\mathcal{L}} + C_{\mathcal{R}})\pi + 140} \tag{28}$$

The solutions for $C_{\mathcal{L}}$ and $C_{\mathcal{R}}$ for a valid double-uniform-PM distribution can also be determined by evaluating the following expressions for specified values of τ_3 and τ_4:

$$C_{\mathcal{L}} = \frac{2(16\tau_3 - 35\tau_4)}{3\pi(7\tau_4 - 2)} \tag{29}$$

$$C_{\mathcal{R}} = \frac{2(16\tau_3 + 35\tau_4)}{3\pi(2 - 7\tau_4)} \tag{30}$$

3.3 *L*-Moment-Based Double-Triangular-PM Distributions

The L-moment-based system of equations for the double-triangular-PM

distributions can be derived by first defining the PWMs based on (20) in terms of $p(T)$ in (5) and then by integrating the following integral:

$$\beta_r = \int_{-\sqrt{2\pi}}^{0} (t + C_{\mathcal{L}} t^3)\{\Phi(t)\}^r \phi(t) dt + \int_{0}^{\sqrt{2\pi}} (t + C_{\mathcal{R}} t^3)\{\Phi(t)\}^r \phi(t) dt. \quad (31)$$

where $\phi(t)$ and $\Phi(t)$ are the standard triangular pdf and cdf given as:

$$\phi(t) = \begin{cases} \left(\sqrt{2\pi} + t\right)/2\pi\,, & \text{for } t \le 0 \\ \left(\sqrt{2\pi} - t\right)/2\pi\,, & \text{for } t > 0 \end{cases} \quad \text{and}$$

$$\Phi(t) = \begin{cases} \left(\sqrt{2\pi} + t\right)^2/4\pi\,, & \text{for } t \le 0 \\ 1 - \left(\sqrt{2\pi} - t\right)^2/4\pi\,, & \text{for } t > 0 \end{cases}.$$

Integrating (31) for $\beta_{r=0,1,2,3}$ and substituting into (16)—(19) yields the first four L-moments; which are eventually substituted into (21)—(22) to obtain the following system of equations:

$$\lambda_1 = \frac{(C_{\mathcal{R}} - C_{\mathcal{L}})\pi^{3/2}}{5\sqrt{2}} \quad (32)$$

$$\lambda_2 = \frac{\sqrt{\pi}\left(49 + 18\pi(C_{\mathcal{L}} + C_{\mathcal{R}})\right)}{105\sqrt{2}} \quad (33)$$

$$\tau_3 = \frac{53\pi(C_{\mathcal{R}} - C_{\mathcal{L}})}{72\pi(C_{\mathcal{L}} + C_{\mathcal{R}}) + 196} \quad (34)$$

$$\tau_4 = \frac{1116\pi(C_{\mathcal{L}} + C_{\mathcal{R}}) + 583}{2376\pi(C_{\mathcal{L}} + C_{\mathcal{R}}) + 6468} \quad (35)$$

The solutions for $C_{\mathcal{L}}$ and $C_{\mathcal{R}}$ for a valid double-triangular-PM distribution can also be determined by evaluating the following expressions for specified values of τ_3 and τ_4:

$$C_{\mathcal{L}} = \frac{(30899 + 176760\tau_3 - 342804\tau_4)}{3816\pi(66\tau_4 - 31)} \quad (36)$$

$$C_{\mathcal{R}} = \frac{(30899 - 176760\tau_3 - 342804\tau_4)}{3816\pi(66\tau_4 - 31)} \quad (37)$$

For specified values of L-skew (τ_3) and L-kurtosis (τ_4) associated with the valid double-uniform-PM and double-triangular-PM distributions, the systems of equations (27)—(28) and (34)—(35) can be simultaneously solved for the values

of shape parameters ($C_{\mathcal{L}}$ and $C_{\mathcal{R}}$). Alternatively, the specified values of L-skew (τ_3) and L-kurtosis (τ_4) associated with the valid double-uniform-PM and double-triangular-PM distributions can be directly substituted into (29)—(30) and (36)—(37), respectively, to obtain the values of $C_{\mathcal{L}}$ and $C_{\mathcal{R}}$. The solved values of $C_{\mathcal{L}}$ and $C_{\mathcal{R}}$ can be substituted into (4) and (5), respectively, for generating the double-uniform-PM and double-triangular-PM distributions. Further, the solved values of $C_{\mathcal{L}}$ and $C_{\mathcal{R}}$ can be substituted into (25)—(26) and (32)—(33) to determine the values of L-location (λ_1) and L-scale (λ_2) associated with the double-uniform-PM and double-triangular-PM distributions, respectively.

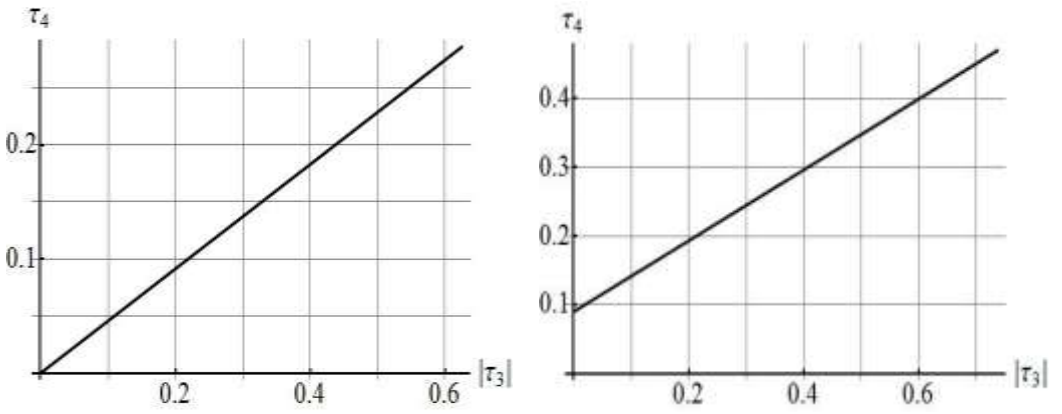

A B

Figure 4: Boundary graphs of the regions for possible combinations of (absolute value) L-skew ($|\tau_3|$) and L-kurtosis (τ_4) for the symmetric double-uniform-PM (Panel A) and the double-triangular-PM (Panel B) distributions.

The boundary graphs in Figure 4 (Panel A and Panel B) can be used for finding possible combinations of L-skew (τ_3) and L-kurtosis (τ_4) associated with the L-moment-based valid double-uniform-PM and double-triangular-PM distributions. Figure 4 (Panel A) shows the boundary graph for possible combinations of L-skew (τ_3) and L-kurtosis (τ_4) associated with a valid double-uniform-PM distribution, where the values of $|\tau_3|$ range between 0 and

0.625 and those of τ_4 range between 0 and 0.2857. Figure 4 (Panel B) shows the boundary graph for possible combinations of L-skew (τ_3) and L-kurtosis (τ_4) associated with a valid double-triangular-PM distribution, where the values of $|\tau_3|$ range between 0 and 0.7361 and those of τ_4 range between 0.0901 to 0.4697.

In the next section, examples are provided to demonstrate the aforementioned methodology and the advantages of L-moment-based procedure over the product moment-based procedure in the contexts of fitting data and estimation of parameters.

4 Comparison of L-Moments with Product Moments

4.1 Fitting Data

Provided in Figure 5 (Panels A and B) are the pdfs of the product moment- and the L-moment-based double-triangular-PM distributions superimposed on the histogram of Thigh circumference data associated with 252 men from the dataset "bodyfat," which was downloaded from http://lib.stat.cmu.edu/datasets/bodyfat.

The product moment-based estimates ($\hat{\gamma}_3$ and $\hat{\gamma}_4$) of skew and kurtosis (γ_3 and γ_4) and the L-moment-based estimates ($\hat{\tau}_3$ and $\hat{\tau}_4$) of L-skew and L-kurtosis (τ_3 and τ_4) were computed for the sample of $n = 252$. The estimates $\hat{\gamma}_3$ and $\hat{\gamma}_4$ were computed using Fisher's k-statistics formulae [33, pages 47-48], whereas the estimates $\hat{\tau}_3$ and $\hat{\tau}_4$ were computed by substituting sample estimates of PWMs from (23) into (16)−(19) for obtaining the sample estimates of L-moments and subsequently substituting these estimates of L-moments into the formulae for the estimates $\hat{\tau}_3$ and $\hat{\tau}_4$. The sample estimates ($\hat{\gamma}_3$, $\hat{\gamma}_4$ and $\hat{\tau}_3$, $\hat{\tau}_4$) were then substituted into the left-hand sides of (A) (14)—(15) and (B) (34)—(35), respectively, to simultaneously solve for the values of shape parameters ($C_{\mathcal{L}}$ and $C_{\mathcal{R}}$) associated with the product moment- and the

L-moment-based double-triangular-PM distributions. The solved values of $C_{\mathcal{L}}$ and $C_{\mathcal{R}}$ were finally substituted into (5) and (3) to superimpose the parametric plots of the double-triangular-PM pdfs shown in Figure 5 (Panels A and B).

Table 3: Chi-square goodness of fit statistics for the product moment-based (P) and the L-moment-based (L) double-triangular-PM approximations for the Thigh circumference data $(n = 252)$ shown in Figure 5 (Panels A and B).

Percent	Expected	Obs. (P)	Obs. (L)	Class Intervals (P)	Class Intervals (L)
10	25.2	33	27	< 53.8020	< 53.0657
20	25.2	33	25	53.8020 – 56.2285	53.0657 – 55.2394
30	25.2	26	21	56.2285 – 57.4936	55.2394 – 56.7618
40	25.2	14	28	57.4936 – 58.3147	56.7618 – 57.9854
50	25.2	19	26	58.3147 – 58.9499	57.9854 – 59.0419
60	25.2	15	23	58.9499 – 59.5959	59.0419 – 60.1070
70	25.2	17	26	59.5959 – 60.5107	60.1070 – 61.4054
80	25.2	30	20	60.5107 – 62.1242	61.4054 – 63.2059
90	25.2	38	34	62.1242 – 65.6385	63.2059 – 66.2480
100	25.2	27	22	65.6385 or greater	66.2480 or greater
				$\chi^2 = 25.6984$	$\chi^2 = 5.9365$
				$p = 0.0001$	$p = 0.3124$

Inspection of Figure 5 (Panels A and B) illustrates that the L-moment-based double-triangular-PM pdf provides a better fit to the Thigh circumference data. The Chi-Square goodness of fit statistics along with their corresponding p-values given in Table 3 provide evidence that the product moment-based

double-triangular-PM distribution does not provide a good fit to the Thigh circumference data, whereas, the L -moment-based double-triangular-PM distribution fits very well. The degrees of freedom for the Chi-Square goodness of fit tests were computed as df = 5 = 10 (class intervals) – 4 (estimates of the parameters) – 1 (sample size).

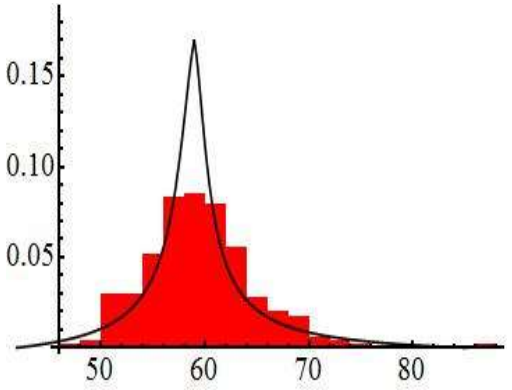

Product moment-based double-triangular-PM pdf superimposed on the histogram of Thigh circumference data $(n = 252)$.

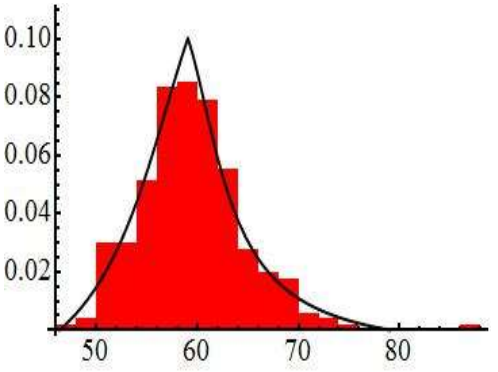

L-moment-based double-triangular-PM pdf superimposed on the histogram of Thigh circumference data $(n = 252)$.

Estimates	Parameters
$\bar{X} = 59.405952$	$\mu = 0.194003$
$s = 5.249952$	$\sigma = 2.233446$
$\hat{\gamma}_3 = 0.821210$	$C_{\mathcal{L}} = 0.302371$
$\hat{\gamma}_4 = 2.665714$	$C_{\mathcal{R}} = 0.548730$

A

Estimates	Parameters
$\hat{\lambda}_1 = 59.405952$	$\lambda_1 = 0.091460$
$\hat{\lambda}_2 = 2.873963$	$\lambda_2 = 0.722054$
$\hat{\tau}_3 = 0.079921$	$C_{\mathcal{L}} = 0.043542$
$\hat{\tau}_4 = 0.162244$	$C_{\mathcal{R}} = 0.159684$

B

Figure 5: The pdfs of (A) product moment- and (B) L -moment-based double-triangular-PM distributions superimposed on histograms of the Thigh circumference data. To superimpose the double-triangular-PM distributions, the piecewise function $p(T)$ from (5) was transformed as (A) $\bar{X} + s\,(p(T) - \mu)/\sigma$ and (B) $\hat{\lambda}_1 + \hat{\lambda}_2\,(p(T) - \lambda_1)/\lambda_2$, respectively, where $(\bar{X},\ s)$ and $(\mu,\ \sigma)$ are the values of (mean, standard deviation), whereas $(\hat{\lambda}_1,\ \hat{\lambda}_2)$ and $(\lambda_1,\ \lambda_2)$ are the values of (L-mean, L-scale) obtained from the actual data and the double-triangular-PM distribution, respectively.

4.2 Estimation of Parameters

In the context of estimation of parameters, an example is provided in Figure 6 and Tables 4 and 5 to demonstrate the advantages of L-moment-based procedure over the product moment-based procedure. Given in Figure 6 (Panel A) are the pdfs of four distributions of which the first and third (Distributions 1 and 3) are the double-uniform-PM and the second and fourth (Distributions 2 and 4) are the double-triangular-PM distributions. Distributions 1 and 2 are symmetric and Distributions 3 and 4 are asymmetric distributions. The values of product moment- and L-moment-based parameters of skew (γ_3), kurtosis (γ_4) and L-skew (τ_3), L-kurtosis (τ_4) along with their solved values of shape parameters $(C_{\mathcal{L}}$ and $C_{\mathcal{R}})$ associated with these four distributions, are provided in Figure 6 (Panel B). The pdfs in Figure 6 (Panel A) were plotted by first substituting the solved values of $C_{\mathcal{L}}$ and $C_{\mathcal{R}}$ into (4) and (5), respectively, to generate the double-uniform-PM and double-triangular-PM distributions and then substituting these into (3) to plot the parametric forms of pdfs associated with these four distributions.

The advantages of L-moment-based procedure over the product moment-based procedure can be demonstrated in the context of estimation of parameters associated with the four distributions in Figure 6 by considering the Monte Carlo simulation results associated with the indices for the standard error (SE) and percentage of relative bias (RB%) reported in Tables 4 and 5.

Specifically, a Fortran [35] algorithm was written to simulate 25,000 independent samples of sizes $n = 25$ and $n = 500$, and the product moment-based estimates ($\hat{\gamma}_3$ and $\hat{\gamma}_4$) of skew and kurtosis $(\gamma_3$ and $\gamma_4)$ and the L-moment-based estimates ($\hat{\tau}_3$ and $\hat{\tau}_4$) of L-skew and L-kurtosis (τ_3 and τ_4) were computed for each of the $(2 \times 25{,}000)$ samples based on the values of shape parameters ($C_{\mathcal{L}}$ and $C_{\mathcal{R}}$) listed in Figure 6 (Panel B). The estimates ($\hat{\gamma}_3$ and $\hat{\gamma}_4$) of γ_3 and γ_4 were computed based on Fisher's k-statistics formulae [33, pages 47-48], whereas the estimates ($\hat{\tau}_3$ and $\hat{\tau}_4$) of τ_3 and τ_4 were computed by substituting sample estimates of PWMs from (23) into (16)−(19) for

obtaining the sample estimates of L-moments and subsequently substituting these estimates of L-moments into the formulae for the estimates $\hat{\tau}_3$ and $\hat{\tau}_4$. Bias-corrected accelerated bootstrapped average estimates (Estimate), associated 95% confidence intervals (95% C.I.), and standard errors (SE) were obtained for each type of estimates using 10,000 resamples via the commercial software package TIBCO Spotfire S+ [36]. Further, if a parameter was outside its associated 95% C.I., then the percentage of relative bias (RB%) was computed for the estimate as

$$\text{RB\%} = 100 \times (\text{Estimate} - \text{Parameter})/\text{Parameter} \tag{38}$$

Table 4: Parameter values of product moment-based skew (γ_3) and kurtosis (γ_4), their corresponding bootstrap estimates, associated 95% confidence intervals (95% C.I.), and standard errors (SE) for the four distributions in Figure 6. Each bootstrap estimate is based on resampling 25000 statistics. Each statistic is based on sample sizes of 25 and 500.

Dist.	Parameter	Estimate	95% C.I.	SE	RB%
		$n = 25$			
1	$\gamma_3 = 0$	$\hat{\gamma}_3 = 0.0021$	$(-0.0020, 0.0064)$	0.0051	-----
	$\gamma_4 = -0.5$	$\hat{\gamma}_4 = -0.3064$	$(-0.3140, -0.2993)$	0.0243	-38.72
2	$\gamma_3 = 0$	$\hat{\gamma}_3 = 0.0144$	$(-0.0016, 0.0292)$	0.0043	-----
	$\gamma_4 = 4$	$\hat{\gamma}_4 = 3.548$	$(3.5175, 3.5816)$	0.0231	-11.30
3	$\gamma_3 = 1.9$	$\hat{\gamma}_3 = 1.953$	$(1.9450, 1.9603)$	0.0035	2.79
	$\gamma_4 = 2.7$	$\hat{\gamma}_4 = 3.616$	$(3.5763, 3.6638)$	0.0111	33.93
4	$\gamma_3 = 3.33$	$\hat{\gamma}_3 = 2.688$	$(2.6773, 2.6984)$	0.0039	-19.28
	$\gamma_4 = 12.55$	$\hat{\gamma}_4 = 8.217$	$(8.1477, 8.2816)$	0.0079	-34.53

		$n = 500$			
1	$\gamma_3 = 0$	$\hat{\gamma}_3 =$ 0.0002	(-0.0006, 0.0010)	0.0004	-----
	$\gamma_4 = -0.5$	$\hat{\gamma}_4 = -$ 0.4901	(−0.4914, −0.4889)	0.0006	−1.98
2	$\gamma_3 = 0$	$\hat{\gamma}_3 = -$ 0.0014	(−0.0052, 0.0023)	0.0019	-----
	$\gamma_4 = 4$	$\hat{\gamma}_4 =$ 4.001	(3.9937, 4.0101)	0.0041	-----
3	$\gamma_3 = 1.9$	$\hat{\gamma}_3 =$ 1.907	(1.9054, 1.9087)	0.0008	0.37
	$\gamma_4 = 2.7$	$\hat{\gamma}_4 =$ 2.77	(2.7620, 2.7779)	0.0041	2.59
4	$\gamma_3 = 3.33$	$\hat{\gamma}_3 =$ 3.314	(3.3107, 3.3179)	0.0018	−0.48
	$\gamma_4 = 12.55$	$\hat{\gamma}_4 =$ 12.52	(12.4877, 12.5540)	0.0169	-----

Table 5: Parameter values of L-moment-based L-skew (τ_3) and L-kurtosis (τ_4), their corresponding bootstrap estimates, associated 95% confidence intervals (95% C.I.), and standard errors (SE) for the four distributions in Figure 6. Each bootstrap estimate is based on resampling 25000 statistics. Each statistic is based on sample sizes of 25 and 500.

Dist.	Parameter	Estimate	95% C.I.	SE	RB%
		$n = 25$			
1	$\tau_3 = 0$	$\hat{\tau}_3 =$ 0.0004	(−0.0006, 0.0014)	0.0005	-----
	$\tau_4 = 0.1146$	$\hat{\tau}_4 =$ 0.1202	(0.1194, 0.1211)	0.0004	4.89
2	$\tau_3 = 0$	$\hat{\tau}_3 =$ 0.0017	(−0.0008, 0.0040)	0.0012	-----
	$\tau_4 = 0.3773$	$\hat{\tau}_4 =$ 0.3795	(0.3783, 0.3807)	0.0006	0.58
3	$\tau_3 = 0.4909$	$\hat{\tau}_3 =$ 0.4967	(0.4957, 0.4978)	0.0005	1.18
	$\tau_4 = 0.2633$	$\hat{\tau}_4 =$ 0.2888	(0.2871, 0.2904)	0.0009	9.68
4	$\tau_3 = 0.5937$	$\hat{\tau}_3 =$ 0.5727	(0.5711, 0.5742)	0.0008	−3.54
	$\tau_4 = 0.4536$	$\hat{\tau}_4 =$ 0.4678	(0.4660, 0.4694)	0.0009	3.13

			$n = 500$		
1	$\tau_3 = 0$	$\hat{\tau}_3 = 0.0001$	$(-0.0001, 0.0002)$	0.0001	-----
	$\tau_4 = 0.1146$	$\hat{\tau}_4 = 0.1149$	$(0.1146, 0.1150)$	0.0001	-----
2	$\tau_3 = 0$	$\hat{\tau}_3 = -0.0002$	$(-0.0006, 0.0004)$	0.0003	-----
	$\tau_4 = 0.3773$	$\hat{\tau}_4 = 0.3775$	$(0.3772, 0.3777)$	0.0001	-----
3	$\tau_3 = 0.4909$	$\hat{\tau}_3 = 0.4914$	$(0.4912, 0.4916)$	0.0001	0.10
	$\tau_4 = 0.2633$	$\hat{\tau}_4 = 0.2647$	$(0.2644, 0.2651)$	0.0002	0.53
4	$\tau_3 = 0.5937$	$\hat{\tau}_3 = 0.5931$	$(0.5929, 0.5933)$	0.0001	-0.10
	$\tau_4 = 0.4536$	$\hat{\tau}_4 = 0.4546$	$(0.4542, 0.4549)$	0.0002	0.22

The results in Tables 4 and 5 illustrate that the L-moment-based estimators are superior to their product moment-based counterparts in terms of both smaller relative bias and error. These characteristics are most pronounced in the context of smaller sample sizes and higher-order moments. For example for the Distribution 4, given a sample size of 25, the product moment-based estimates ($\hat{\gamma}_3$ and $\hat{\gamma}_4$) generated in the simulation were, on average, 80.72% and 65.47% of their respective parameters (γ_3 and γ_4). On the other hand, for the same Distribution 4, the L-moment-based estimates ($\hat{\tau}_3$ and $\hat{\tau}_4$) generated in the simulation study were, on average, 96.46% and 103.13% of their respective parameters (τ_3 and τ_4). Thus, the relative biases of estimators based on L-moments are essentially negligible compared to those associated with the estimators based on product moments. Also, it can be verified that the standard errors associated with the estimates ($\hat{\tau}_3$ and $\hat{\tau}_4$) are relatively much smaller than the standard errors associated with the estimates ($\hat{\gamma}_3$ and $\hat{\gamma}_4$).

Inspection of the graphs in Figure 5 (Panels A and B) and the Monte Carlo simulation results in Tables 4 and 5 indicate that the L-moment based procedure

is superior to product moment-based procedure in terms of fitting data and estimation of parameters.

Distribution 1
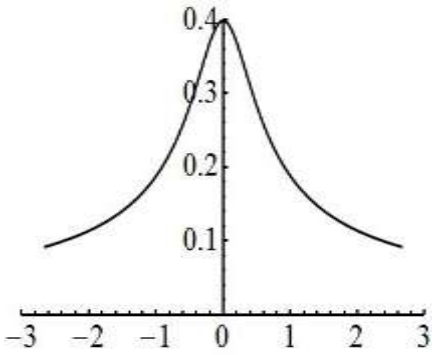 $\gamma_3 = 0,\ \gamma_4 = -0.5$ $(\mu = 0, \sigma = 1.226485)$ $C_{\mathcal{L}} = C_{\mathcal{R}} = 0.710458$ $\tau_3 = 0,\ \tau_4 = 0.1146$ $(\lambda_1 = 0, \lambda_2 = 0.697507)$
Distribution 2
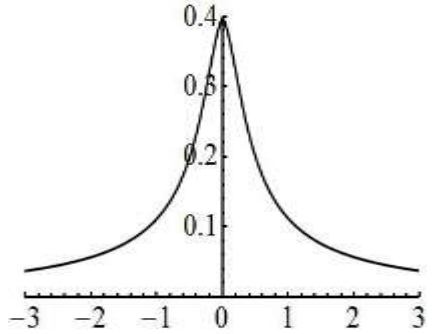 $\gamma_3 = 0,\ \gamma_4 = 4$ $(\mu = 0, \sigma = 4.917699)$ $C_{\mathcal{L}} = C_{\mathcal{R}} = 1.346056$ $\tau_3 = 0,\ \tau_4 = 0.3773$ $(\lambda_1 = 0, \lambda_2 = 2.402011)$
Distribution 3
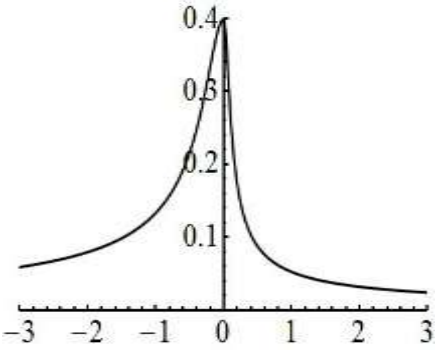 $\gamma_3 = 1.9, \gamma_4 = 2.7$ $(\mu = 5.236402, \sigma = 11.592811)$ $C_{\mathcal{L}} = 1.844870,\ C_{\mathcal{R}} = 23.123476$ $\tau_3 = 0.4909,\ \tau_4 = 0.2633$ $(\lambda_1 = 5.236402, \lambda_2 = 5.333293)$

Distribution 4

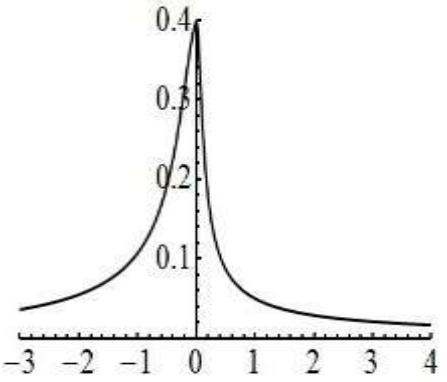

$\gamma_3 = 3.33, \gamma_4 = 12.55$

$(\mu = 12.945011, \sigma = 36.424664)$

$C_{\mathcal{L}} = 1.538219,\ C_{\mathcal{R}} = 17.976736$

$\tau_3 = 0.5937,\ \tau_4 = 0.4536$

$(\lambda_1 = 12.945011, \lambda_2 = 13.757148)$

A B

Figure 6: The pdfs (Panel A) of two double-uniform-PM (Distributions 1 and 3) and two double-triangular-PM (Distributions 2 and 4) distributions, their corresponding parameter values (Panel B) of product moment-based skew (γ_3) and kurtosis (γ_4), L-moment-based L-skew (τ_3) and L-kurtosis (τ_4), and the solved values of shape parameters ($C_{\mathcal{L}}$ and $C_{\mathcal{R}}$).

5 L -Correlations for the Double-Uniform-PM and Double-Triangular-PM Distributions

Let Y_j and Y_k be two random variables with cdf s $F(Y_j)$ and $F(Y_k)$ respectively. The second L-moments of Y_j and Y_k can be defined as [37]:

$$\lambda_2(Y_j) = 2Cov\left(Y_j, F(Y_j)\right) \tag{39}$$

$$\lambda_2(Y_k) = 2Cov\left(Y_k, F(Y_k)\right). \tag{40}$$

The second L-comoment of Y_j towards Y_k and Y_k towards Y_j are given as:

$$\lambda_2(Y_j, Y_k) = 2Cov\left(Y_j, F(Y_k)\right) \tag{41}$$

$$\lambda_2(Y_k, Y_j) = 2Cov\left(Y_k, F(Y_j)\right). \tag{42}$$

The L-correlations of Y_j toward Y_k and Y_k toward Y_j are subsequently

defined as:

$$\eta_{jk} = \frac{\lambda_2(Y_j, Y_k)}{\lambda_2(Y_j)} \tag{43}$$

$$\eta_{kj} = \frac{\lambda_2(Y_k, Y_j)}{\lambda_2(Y_k)} \tag{44}$$

The L-correlation given in (43) (or, 44) is bounded such that $-1 \leq \eta_{jk} \leq 1$. A value of $\eta_{jk} = 1$ $(\text{or}, \eta_{jk} = -1)$ implies that Y_j and Y_k have a strictly and monotonically increasing (or, decreasing) relationship. See Serfling and Xiao [37] for further details on the topics related with L-correlation.

The extension of the double-uniform-PM and double-triangular-PM distributions to multivariate level can be achieved by specifying T piecewise functions as given in (4) and/or (5) with a specified L-correlation structure. Specifically, let $Z_1, \ldots, Z_T$ denote standard normal variables with cdfs and the joint pdf associated with Z_j and Z_k given by the following expressions:

$$\Phi(Z_j) = \int_{-\infty}^{z_j} (2\pi)^{-1/2} \exp\{-v_j^2/2\}\, dv_j \tag{45}$$

$$\Phi(Z_k) = \int_{-\infty}^{z_k} (2\pi)^{-1/2} \exp\{-v_k^2/2\}\, dv_k \tag{46}$$

$$f_{jk} = \left(2\pi\left(1 - r_{jk}^2\right)^{1/2}\right)^{-1} \exp\left\{-\left(2\left(1 - r_{jk}^2\right)\right)^{-1} \left(z_j^2 + z_k^2 - 2r_{jk} z_j z_k\right)\right\}. \tag{47}$$

where r_{jk} in (47) is the intermediate correlation between Z_j and Z_k. The cdfs in (45) and (46) are considered as zero-one uniform deviates, i.e., $\Phi(Z_j), \Phi(Z_k) \sim Unif(0,1)$. These zero-one uniform deviates can be transformed into $U \sim Unif(-\sqrt{\pi/2}, \sqrt{\pi/2})$ and $T \sim Tri(-\sqrt{2\pi}, \sqrt{2\pi})$ variates for the functions defined in (4) and (5) as:

$$U = \sqrt{\pi/2}\,(2\Phi(Z) - 1), \tag{48}$$

$$T = \begin{cases} \sqrt{2\pi}\left(\sqrt{2\Phi(Z)} - 1\right), & \text{for } \Phi(Z) \leq 0.5 \\ \sqrt{2\pi}\left(1 - \sqrt{2\left(1 - \Phi(Z)\right)}\right), & \text{for } \Phi(Z) > 0.5 \end{cases} \tag{49}$$

As such, the piecewise functions $p(U)$ in (4) and $p(T)$ in (5) can be considered as functions of $\Phi(Z_j)$, or $\Phi(Z_k)$ $\left(\text{e.g., } p_j\left(\Phi(Z_j)\right) \text{ or } p_k\left(\Phi(Z_k)\right)\right)$. Thus, the L-correlation of $Y_j = p_j\left(\Phi(Z_j)\right)$ toward $Y_k = p_k\left(\Phi(Z_k)\right)$ can be determined using (43) with the denominator standardized to $\lambda_2(Y_j) = 1/\sqrt{\pi}$ for the standard normal distribution as:

$$\eta_{jk} = 2\sqrt{\pi}\int_{-\infty}^{\infty}\int_{-\infty}^{\infty} x_j\left(p_j\left(\Phi(Z_j)\right)\right)\Phi(z_k)\, f_{jk}\, dz_j dz_k. \tag{50}$$

The variable $x_j\left(p_j\left(\Phi(Z_j)\right)\right)$ in (50) is the standardized piecewise function defined in (4) or (5) such that it has a L-location (or, mean) of zero and L-scale equal to that of the standard normal distribution. That is, the quantile function $Y_j = p_j\left(\Phi(Z_j)\right)$ is standardized by a linear transformation as:

$$x_j\left(p_j\left(\Phi(Z_j)\right)\right) = \xi\left(p_j\left(\Phi(Z_j)\right) - \lambda_1\right) \tag{51}$$

where λ_1 is the mean from (25) or (32) and ξ is a constant that scales λ_2 in (26) or (33) and in the denominator of (43) to $1/\sqrt{\pi}$. In particular, ξ for the double-uniform-PM and double-triangular-PM distributions can be expressed as:

$$\xi_{(\text{double-uniform-PM})} = \frac{60\sqrt{2}}{\pi(20 + 3\pi C_{\mathcal{L}} + 3\pi C_{\mathcal{R}})} \tag{52}$$

$$\xi_{(\text{double-triangular-PM})} = \frac{105\sqrt{2}}{\pi(49 + 18\pi C_{\mathcal{L}} + 18\pi C_{\mathcal{R}})}. \tag{53}$$

The next step is to use (50) to solve for the values of the $n(n-1)/2$ intermediate correlations (r_{jk}) such that the n specified double-uniform-PM

and/or double-triangular-PM distributions have their specified L-correlation structure.

Analogously, the L-correlation of $Y_k = p_k\big(\Phi(Z_k)\big)$ toward $Y_j = p_j\left(\Phi\big(Z_j\big)\right)$ is given as

$$\eta_{kj} = 2\sqrt{\pi}\int_{-\infty}^{\infty}\int_{-\infty}^{\infty} x_k\left(p_k\big(\Phi(Z_k)\big)\right)\Phi\big(z_j\big)\, f_{jk}\, dz_k dz_j. \tag{54}$$

Note that in general, the L-correlation of $Y_j = p_j\left(\Phi\big(Z_j\big)\right)$ toward $Y_k = p_k\big(\Phi(Z_k)\big)$ in (50) is not equal to the L-correlation of $Y_k = p_k\big(\Phi(Z_k)\big)$ toward $Y_j = p_j\left(\Phi\big(Z_j\big)\right)$ in (54). These L-correlations are equal only when the values of shape parameters ($C_{\mathcal{L}}$ and $C_{\mathcal{R}}$) associated with $Y_j = p_j\left(\Phi\big(Z_j\big)\right)$ and $Y_k = p_k\big(\Phi(Z_k)\big)$ are equal (i.e., when the two distributions are the same). Source code written in Mathematica [38, 39] is provided in Algorithm 1, which shows an example for computing an intermediate correlation $\big(r_{jk}\big)$ for a specified value of L-correlation. The steps for simulating correlated double-uniform-PM and double-triangular-PM distributions with specified values of L-skew (τ_3), L-kurtosis (τ_4), and with specified L-correlation structure are given in Section 6.

6 The Steps for Monte Carlo Simulation with an Example

The procedure for simulating double-uniform-PM and double-triangular-PM distributions with specified L-moments and L-correlations can be summarized in the following six steps:

1. Specify the L-moments for T transformations of the forms in (4) and (5), i.e., $p_1(U_1), \dots, p_j\big(U_j\big)$, $p_k(T_k), \dots, p_n(T_n)$, where U_j and T_k are the functions of $\Phi(z_j)$ and $\Phi(z_k)$ in (48) and (49), respectively. Obtain the solutions for the shape parameters ($C_{\mathcal{L}}$ and $C_{\mathcal{R}}$) by simultaneously solving the systems of

equations (27)—(28) and (34)—(35) for the specified values of L-skew (τ_3) and L-kurtosis (τ_4) for each distribution. Specify a $n \times n$ matrix of L-correlations (η_{jk}) for $p_j(U_j)$ toward $p_k(T_k)$, where $j < k \in \{1, 2, \ldots, n\}$.

2. Compute the values of intermediate (Pearson) correlations (ICs), r_{jk}, by substituting the value of specified L-correlation (η_{jk}) and the solved values of c and k from Step 1 into the left- and the right-hand sides of (50), respectively, and then numerically integrating (50) to solve for r_{jk}. See Algorithm 1 for an example. Repeat this step separately for all $n(n-1)/2$ pairwise combinations of ICs.
3. Assemble the ICs computed in Step 2 into a $n \times n$ matrix and then decompose this matrix using Cholesky factorization. Note that this step requires the IC matrix to be positive definite.
4. Use elements of the matrix resulting from Cholesky factorization of Step 3 to generate n standard normal variables ($Z_1, \ldots, Z_n$) correlated at the IC levels as follows:

$$
\begin{aligned}
Z_1 &= a_{11}V_1 \\
Z_2 &= a_{12}V_1 + a_{22}V_2 \\
&\vdots \\
Z_j &= a_{1j}V_1 + a_{2j}V_2 + \cdots + a_{ij}V_i + \cdots + a_{jj}V_j \\
&\vdots \\
Z_n &= a_{1n}V_1 + a_{2n}V_2 + \cdots + a_{in}V_i + \cdots + a_{jn}V_n + \cdots + a_{nn}V_n
\end{aligned}
\tag{55}
$$

where $V_1, \ldots, V_n$ are independent standard normal random variables and where a_{ij} is the element in the i-th row and j-th column of the matrix resulting from Cholesky factorization of Step 3.

5. Substitute $Z_1, \ldots, Z_n$ from Step 4 into the following Taylor series-based expansion for computing the cdf, $\Phi(Z_j)$, of standard normal distribution [40]

$$\Phi(Z_j) = 0.5 + \phi(Z_j)\{Z_j + Z_j^3/3 + Z_j^5/(3 \cdot 5) + Z_j^7/(3 \cdot 5 \cdot 7) + \cdots\} \quad (56)$$

where $\phi(Z_j)$ is the pdf of standard normal distribution and the absolute error associated with (56) is less than 8×10^{-16}.

6. Substitute the uniform (0, 1) variables, $\Phi(Z_j)$, generated in Step 5 into (48) and (49) for obtaining the $Unif(-\sqrt{\pi/2}, \sqrt{\pi/2})$ and $Tri(-\sqrt{2\pi}, \sqrt{2\pi})$ deviates, which are subsequently substituted into n equations of the form in (4) and (5) to generate the double-uniform-PM and double-triangular-PM distributions with specified values of L-skew (τ_3), L-kurtosis (τ_4), and with specified L-correlation structure.

For the purpose of evaluating the proposed methodology and demonstrating the steps above, an example is subsequently provided to compare the L-moment-based L-correlation procedure with the product moment-based Pearson correlation procedure. Specifically, the distributions in Fig. 6 are used as a basis for a comparison using the specified correlation matrix in Table 6 where strong, moderate, and weak correlations are considered in a single matrix. Let the four distributions in Fig. 6 be $Y_1 = p_1(U_1)$, $Y_2 = p_2(T_2)$, $Y_3 = p_3(U_3)$, and $Y_4 = p_4(T_4)$, respectively, from (4) and (5), where U_1 and U_3 are the functions of $\Phi(Z_1)$ and $\Phi(Z_3)$ based on (48) and T_2 and T_4 are the functions of $\Phi(Z_2)$ and $\Phi(Z_4)$ based on (49). The specified values of product moment-based skew (γ_3) and kurtosis (γ_4) and L-moment-based L-skew (τ_3) and L-kurtosis (τ_4) along with the solved values of shape parameters associated with these four distributions are given in Fig. 6 (Panel B). Provided in Tables 7 and 8 are the intermediate correlations (IC s) obtained, respectively, for the product moment-based Pearson correlation and L -moment-based L -correlation procedures for the distributions in Figure 6. Provided in Algorithm 2 is a source

code written in Mathematica [38, 39], which shows an example for computing ICs for the product moment-based Pearson correlation procedure. See Appendix for a description of methodology on simulating Pearson correlation based multivariate distributions. See, also Pant and Headrick [24, pages 6474-6475] for a detailed methodology for simulating correlated double-PM distributions through the method of Pearson correlation.

Provided in Tables 9 and 10 are the results of Cholesky factorization on the IC matrices in Tables 7 and 8, respectively. The elements of matrices in Tables 9 and 10 are used to generate $Z_1, \ldots, Z_4$ correlated at the IC levels by making use of the formulae (55) in Step 4 with $n = 4$. The values of $Z_1, \ldots, Z_4$ are then used in (56) to obtain the Taylor series-based approximations of the cdfs $\Phi(Z_1)$, $\Phi(Z_2)$, $\Phi(Z_3)$, and $\Phi(Z_4)$, which are treated as $U(0,1)$. These zero-one uniform deviates are substituted into (48) and (49) to obtain the $Unif(-\sqrt{\pi/2}, \sqrt{\pi/2})$ and $Tri(-\sqrt{2\pi}, \sqrt{2\pi})$ variates, which are finally substituted into (4) and (5) to generate the four distributions in Figure 6 that are correlated at the specified correlation level of Table 6.

For the Monte Carlo simulation, a Fortran [35] algorithm was written for both procedures to generate 25,000 independent sample estimates for the specified parameters of (a) product moment-based skew (γ_3), kurtosis (γ_4), and Pearson correlation (ρ_{jk}), and (b) L-moment-based L-skew (τ_3), L-kurtosis (τ_4), and L-correlation (η_{jk}) based on samples of sizes $n = 25$ and $n = 500$. The estimates of γ_3 and γ_4 were computed using the Fisher's k-statistics formulae [33, pages 47-48], which are currently used by most commercial software packages such as SAS, SPSS, Minitab, etc., for computing the values of skew and kurtosis (where $\gamma_{3,4} = 0$ for the standard normal distribution). The estimate for ρ_{jk} was based on the usual formula for the Pearson correlation statistic. The estimate of η_{jk} was computed by substituting (39) and (41) into (43), where the empirical forms of the cdfs were used in (39) and (41). The sample estimates

ρ_{jk} and η_{jk} were both transformed using Fisher's z' transformations. Bias-corrected accelerated bootstrapped average estimates (Estimate), associated 95% confidence intervals (95% C. I.), and standard errors (SE) were obtained for the estimates associated with the parameters $\left(\gamma_{3,4}, \tau_{3,4}, z'_{(\rho_{jk})}, z'_{(\eta_{jk})}\right)$ using 10,000 resamples via the commercial software package TIBCO Spotfire S+ [36]. The bootstrap results associated with the estimates of $z'_{(\rho_{jk})}$ and $z'_{(\eta_{jk})}$ were transformed back to their original metrics. Further, if a parameter was outside its associated 95% C.I., then an index of relative bias (RB%) was computed for the estimate using (38). The results of this simulation are presented in Tables 4, 5, 11, 12, and are discussed in the next section.

Table 6: Specified correlations for the four distributions in Figure 6.

Distribution	1	2	3	4
1	1.0			
2	0.75	1.0		
3	0.65	0.45	1.0	
4	0.55	0.40	0.35	1.0

Table 7: Intermediate correlations for the product moment-based Pearson correlation procedure.

	1	2	3	4
1	1.0			
2	0.815205	1.0		
3	0.780825	0.567608	1.0	
4	0.756481	0.550618	0.466007	1.0

Table 8: Intermediate correlations for the L-moment-based L-correlation procedure.

	1	2	3	4
1	1.0			
2	0.753655	1.0		
3	0.654484	0.419888	1.0	
4	0.554824	0.372290	0.341364	1.0

Table 9: Cholesky decomposition on the intermediate correlations matrix of Table 7.

$a_{11} = 1.0$	$a_{12} = 0.815205$	$a_{13} = 0.780825$	$a_{14} = 0.756481$
$a_{21} = 0.0$	$a_{22} = 0.579173$	$a_{23} = -0.119004$	$a_{24} = -0.114075$
$a_{31} = 0.0$	$a_{32} = 0.0$	$a_{33} = 0.613311$	$a_{34} = -0.225412$
$a_{41} = 0.0$	$a_{42} = 0.0$	$a_{43} = 0.0$	$a_{44} = 0.603252$

Table 10: Cholesky decomposition on the intermediate correlations matrix of Table 8.

$a_{11} = 1.0$	$a_{12} = 0.753655$	$a_{13} = 0.654484$	$a_{14} = 0.554824$
$a_{21} = 0.0$	$a_{22} = 0.657271$	$a_{23} = -0.111623$	$a_{24} = -0.069768$
$a_{31} = 0.0$	$a_{32} = 0.0$	$a_{33} = 0.747791$	$a_{34} = -0.039513$
$a_{41} = 0.0$	$a_{42} = 0.0$	$a_{43} = 0.0$	$a_{44} = 0.828095$

7 Discussion and Conclusion

The advantages of L-moment-based procedure over the product

moment-based procedure can be expressed in the context of fitting real-world data, estimation of parameters, and simulating correlated non-normal distributions with specified correlations.

One of the advantages of L-moment-based procedure can be highlighted in the context of fitting real-world data. Comparison of the two distributions in Figure 5 (Panels A and B) clearly indicates that L-moment-based double-triangular-PM distribution (Fig. 5, Panel B) provides a better fit to the Thigh circumference data, whereas the product moment-based double-triangular-PM distribution (Fig. 5, Panel A) does not provide a good fit to the data.

Another advantage of the L-moment-based procedure over product moment-based procedure can be expressed in the context of estimation. The L-moment-based estimators of L-skew and L-kurtosis can be far less biased than the product moment based estimators of skew and kurtosis when samples are drawn from the distributions with more severe departures from normality [22-24, 29-31, 32, 34]. Inspection of the simulation results in Tables 4 and 5 clearly indicates the superiority that estimates ($\hat{\tau}_3$ and $\hat{\tau}_4$) of L-skew (τ_3) and L-kurtosis (τ_4) have over their corresponding product moment-based estimates ($\hat{\gamma}_3$ and $\hat{\gamma}_4$) of skew (γ_3) and kurtosis (γ_4) in terms of less bias and dispersion in the context of double-uniform-PM and double-triangular-PM distributions. For example, for samples of size $n = 25$, the estimates $\hat{\tau}_3$ and $\hat{\tau}_4$ for Distribution 4 were, on average, 96.46% and 103.13% of their corresponding parameters, whereas the estimates $\hat{\gamma}_3$ and $\hat{\gamma}_4$ were 80.72% and 65.47% of their corresponding parameters.

Another advantage that L-moment-based estimates have over their product moment-based counterparts can be expressed by comparing their relative standard errors (RSEs) defined as $\text{RSE} = \{(\text{SE}/\text{Estimate}) \times 100\}$. Comparing Tables 4 and 5, it is evident that the estimates of τ_3 and τ_4 are more efficient as their RSEs are considerably smaller than the RSEs associated with the product moment-based estimates of γ_3 and γ_4. For example, in terms of Distribution 4 in

Figure 6, inspection of Tables 4 and 5 (for $n = 500$), indicates that RSE measures of: RSE $(\hat{\tau}_3) = 0.017\%$ and RSE $(\hat{\tau}_4) = 0.044\%$ are considerably smaller than the RSE measures of: RSE $(\hat{\gamma}_3) = 0.054\%$ and RSE $(\hat{\gamma}_4) = 0.135\%$. Additionally, in terms of distribution in Fig. 2A, inspection of Tables 1 and 2 (for $n = 25$), indicates that RSE measures of: RSE $(\hat{\tau}_3) = 0.185\%$ and RSE $(\hat{\tau}_4) = 0.262\%$ are considerably smaller than the RSE measures of: RSE $(\hat{\gamma}_3) = 0.235\%$ and RSE $(\hat{\gamma}_4) = 0.753\%$. This demonstrates that the estimates of L-skew and L-kurtosis have higher precision compared to estimates of skew and kurtosis because the former have less variance around their bootstrapped estimates than the latter.

Presented in Tables 11 and 12 are the simulation results of product moment-based Pearson correlations and L-correlations, respectively. Overall inspection of these tables indicates that the L-correlation is superior to Pearson correlation in terms of relative bias. For example, for $n = 25$, the relative bias for the two distributions, Distributions 1 and 4, in Figure 6 was 6.78% for the Pearson correlation compared with only 2.11% for the L-correlation. It is also noted that the variability associated with bootstrapped estimates of L-correlation appears to be more stable than that of the bootstrapped estimates of Pearson correlation both within and across different conditions.

In summary, the new L-moment-based procedure is an attractive alternative to the more traditional product moment-based procedure in the context of the two families of double-uniform-PM and double-triangular-PM distributions. In particular, the L-moment-based procedure has distinct advantages when distributions with large departures from normality are used. Finally, we note that Mathematica [38, 39] source codes are available from the authors for implementing both the L-moment- and product moment-based procedures.

(* Intermediate Correlation *)

$r_{34} = 0.341364;$

$f_{34} =$ PDF[MultinormalDistribution[{0, 0}, {{1, r_{34}}, {r_{34}, 1}}], {Z_3, Z_4}];

$\Phi_3 =$ CDF[NormalDistribution[0, 1], Z_3];

$\Phi_4 =$ CDF[NormalDistribution[0, 1], Z_4];

(* Shape parameters for Distribution 3 in Figure 6 (Panel A). The values of L-location (λ_1) and the normalizing constant (ξ_1) were based on equations (25) and (52) *)

$C_{\mathcal{L}} = 1.844870;$

$C_{\mathcal{R}} = 23.123476;$

$\lambda_1 = 5.236402;$

$\xi_1 = 0.105786;$

$X_3 = \sqrt{\pi/2}\,(2\Phi_3 - 1)$

$YL_3 = X_3 + C_{\mathcal{L}} * X_3^3;$

$YR_3 = X_3 + C_{\mathcal{R}} * X_3^3;$

(* The piecewise function based on equation (4), which is Distribution 3 in Figure 6 (Panel A) *)

$Y_3 =$ Piecewise[{{$YL_3, X_3 \leq 0$}, {$YR_3, X_3 > 0$}}];

(* Standardize Distribution 3 in Figure 6 (Panel A) *)

$x_3 = \xi_1 * (Y_3 - \lambda_1);$

(* Compute the specified L-correlation *)

$\eta_{34} = 2\sqrt{\pi} *$ NIntegrate[$x_3 * \Phi_4 * f_{34}$, { Z_3 , -8, 8}, { Z_4 , -8, 8}, Method → MultiDimensional]

0.349999

Algorithm 1: Mathematica algorithm for computing intermediate correlations (ICs) for specified values of L-correlations. The example is for L-correlation of Distribution $j = 3$ toward Distribution $k = 4$ (η_{34}). See Distributions 3 and 4 in Figure 6 (Panel A), specified correlation in Table 6, and intermediate correlation in Table 8.

(* Intermediate Correlation *)

$r_{34} = 0.466007;$

$f_{34} =$ PDF[MultinormalDistribution[{0, 0}, {{1, r_{34}}, {r_{34}, 1}}], {Z_3, Z_4}];

$\Phi_3 =$ CDF[NormalDistribution[0, 1], Z_3];

$\Phi_4 =$ CDF[NormalDistribution[0, 1], Z_4];

(* Parameters for Distributions 3 and 4 in Fig. 6 (Panel A) *)

$C_{\mathcal{L}3} = 1.844870;$

$C_{\mathcal{R}3} = 23.123476;$

$\mu_3 = 5.236402;$

$\sigma_3 = 11.592811;$

$C_{\mathcal{L}4} = 1.538219;$

$C_{\mathcal{R}4} = 17.976736;$

$\mu_4 = 12.945011;$

$\sigma_4 = 36.424664;$

$X_3 = \sqrt{\pi/2}\,(2\Phi_3 - 1);$

$X_4 =$ Piecewise[{{$\sqrt{2\pi}(\sqrt{2\Phi_4} - 1), \Phi_4 \leq 0.5$}, {$\sqrt{2\pi}(1 - \sqrt{2(1 - \Phi_4)}), \Phi_4 > 0.5$}}];

$YL_3 = X_3 + C_{\mathcal{L}3} * X_3^3;$

$YR_3 = X_3 + C_{\mathcal{R}3} * X_3^3;$

$YL_4 = X_4 + C_{\mathcal{L}4} * X_4^3;$

$YR_4 = X_4 + C_{\mathcal{R}4} * X_4^3;$

(* Distributions 3 and 4 in Fig. 6 (Panel A) based on equations (4) and (5) *)

$Y_3 = \text{Piecewise}[\{\{YL_3, X_3 \leq 0\}, \{YR_3, X_3 > 0\}\}];$
$Y_4 = \text{Piecewise}[\{\{YL_4, X_4 \leq 0\}, \{YR_4, X_4 > 0\}\}];$

(* Standardize each distribution *)
$x_3 = (Y_3 - \mu_3)/\sigma_3;$
$x_4 = (Y_4 - \mu_4)/\sigma_4;$

(* Compute the specified product moment-based Pearson correlation *)
$\rho_{34} = \text{NIntegrate}[x_3 * x_4 * f_{34}, \{Z_3, -8, 8\}, \{Z_4, -8, 8\}, \text{Method} \rightarrow \text{MultiDimensional}]$

0.35

Algorithm 2: Mathematica algorithm for computing intermediate correlations (ICs) for specified product moment-based Pearson correlations. The example is for Pearson correlation between Distribution $j = 3$ and Distribution $k = 4$ (ρ_{34}). See pdfs of Distributions 3 and 4 in Figure 6 (Panel A), specified correlation in Table 6, and intermediate correlation in Table 7.

Table 11: Specified correlations, their corresponding bootstrap estimates, associated 95% confidence intervals (95% C.I.), and standard errors (SE) for the product moment-based Pearson correlations. Each bootstrap estimate is based on resampling 25000 statistics. Each statistic is based on sample sizes of 25 and 500.

Parameter	Estimate	95% C.I.	SE	RB%
		$n = 25$		
$\rho_{12} = 0.75$	0.7641	(0.7630, 0.7649)	0.00117	1.88
$\rho_{13} = 0.65$	0.6627	(0.6614, 0.6640)	0.00116	1.95
$\rho_{14} = 0.55$	0.5873	(0.5860, 0.5888)	0.00108	6.78
$\rho_{23} = 0.45$	0.4680	(0.4656, 0.4701)	0.00146	4.00
$\rho_{24} = 0.40$	0.4262	(0.4237, 0.4288)	0.00157	6.55
$\rho_{34} = 0.35$	0.3770	(0.3737, 0.3803)	0.00198	7.71

		$n = 500$		
$\rho_{12} = 0.75$	0.7506	(0.7504, 0.7508)	0.00025	0.08
$\rho_{13} = 0.65$	0.6501	(0.6498, 0.6503)	0.00024	-----
$\rho_{14} = 0.55$	0.5515	(0.5512, 0.5518)	0.00022	0.27
$\rho_{23} = 0.45$	0.4503	(0.4498, 0.4508)	0.00030	-----
$\rho_{24} = 0.40$	0.4009	(0.4003, 0.4015)	0.00034	0.23
$\rho_{34} = 0.35$	0.3506	(0.3499, 0.3513)	0.00041	-----

Table 12: Specified correlations, their bootstrap estimates along with associated 95% confidence intervals (95% C.I.) and standard errors (SE) for the L-moment-based L-correlation procedure. Each bootstrap estimate is based on resampling 25000 statistics. Each statistic is based on sample sizes of 25 and 500.

Parameter	Estimate	95% C.I.	SE	RB%
		$n = 25$		
$\eta_{12} = 0.75$	0.7610	(0.7597, 0.7621)	0.00143	1.47
$\eta_{13} = 0.65$	0.6616	(0.6601, 0.6632)	0.00140	1.78
$\eta_{14} = 0.55$	0.5616	(0.5595, 0.5634)	0.00142	2.11
$\eta_{23} = 0.45$	0.4603	(0.4578, 0.4627)	0.00161	2.29
$\eta_{24} = 0.40$	0.4065	(0.4039, 0.4091)	0.00159	1.63
$\eta_{34} = 0.35$	0.3651	(0.3619, 0.3681)	0.00179	4.31
		$n = 500$		
$\eta_{12} = 0.75$	0.7504	(0.7502, 0.7507)	0.00030	0.05
$\eta_{13} = 0.65$	0.6499	(0.6496, 0.6503)	0.00030	-----
$\eta_{14} = 0.55$	0.5505	(0.5501, 0.5509)	0.00029	0.09
$\eta_{23} = 0.45$	0.4502	(0.4496, 0.4507)	0.00033	-----
$\eta_{24} = 0.40$	0.4001	(0.3996, 0.4007)	0.00034	-----
$\eta_{34} = 0.35$	0.3500	(0.3495, 0.3507)	0.00036	-----

References

[1] A.I. Fleishman, A method for simulating non-normal distributions, *Psychometrika*, **43**(4), (1978), 521–532.

[2] T.C. Headrick, Fast fifth-order polynomial transforms for generating univariate and multivariate non-normal distributions, *Computational Statistics & Data Analysis*, **40**(4), (2002), 685–711.

[3] T.C. Headrick, *Statistical Simulation: Power Method Polynomials and other Tranformations*, Chapman & Hall/CRC, Boca Raton, FL, USA, 2010.

[4] J. Affleck-Graves and B. MacDonald, Nonnormalities and tests of asset pricing theories, *Journal of Finance*, **44**(4), (1989), 889–908.

[5] H.S. Steyn, On the problem of more than one kurtosis parameter in multivariate analysis, *Journal of Multivariate Analysis*, **44**(1), (1993), 1-22.

[6] G.D. Hess and S. Iwata, Measuring and comparing business-cycle features, *Journal of Business and Economic Statistics*, **15**(4), (1997), 432-444.

[7] D.A. Powell, L.M. Anderson, R.Y. Cheng, and W.G. Alvord, Robustness of the Chen-Dougherty-Bittner procedure against non-normality and heterogeneity distribution in the coefficient of variation, *Journal of Biomedical Optics*, **7**(4), (2002), 650-660.

[8] O. Mahul, Hedging price risk in the presence of crop yield and revenue insurance, *European Review of Agricultural Economics*, **30**(2), (2003), 217–239.

[9] M.R. Harwell and R.C. Serlin, An empirical study of a proposed test of nonparametric analysis of covariance, *Psychological Bulletin*, **104**(2), (1988), 268-281.

[10] T.C. Headrick and S.S. Sawilowsky, Properties of the rank transformation in factorial analysis of covariance, *Communications in Statistics: Simulation and Computation*, **29**(4), (2000),1059–1087.

[11] I. Berkovits, G.R. Hancock, and J. Nevitt, Bootstrap resampling approaches for repeated measures designs: Relative robustness to sphericity and

normality violations, *Educational and Psychological Measurement*, **60**(6), (2000), 877-892.

[12] L.M. Lix and R.T. Fouladi, Robust step-down tests for multivariate independent group designs, *The British Journal of Mathematical and Statistical Psychology*, **60**(2), (2007), 245-265.

[13] H.J. Keselman, R.R. Wilcox, J. Algina, A.R. Othman and K. Fradette, A comparative study of robust tests for spread: asymmetric trimming strategies, *The British Journal of Mathematical and Statistical Psychology*, **61**(2), (2008), 235-253.

[14] T.C. Headrick and O. Rotou, An investigation of the rank transformation in multiple regression, *Computational Statistics & Data Analysis*, **38**(2), (2001), 203-225.

[15] T.M. Beasley and B. D. Zumbo, Comparison of aligned Friedman rank and parametric methods for testing interactions in split-plot designs, *Computational Statistics & Data Analysis*, **42**(4), (2003), 569-593.

[16] C.A. Stone, Empirical power and type I error rates for an IRT fit statistic that considers the precision of ability estimates, *Educational and Psychological Measurement*, **63**(4), (2003), 566-583.

[17] L. Hothorn and W. Lehmacher, A simple testing procedure "control versus *k* treatments" for one-sided ordered alternatives, with application in toxicology, *Biometrical Journal*, **33**(2), (2007), 179–189.

[18] J.M. Henson, S.P. Reise and K.H. Kim, Detecting mixtures from structural model differences using latent variable mixture modeling: A comparison of relative model fit statistics, *Structural Equation Modeling*, **14**(2), (2007), 202-226.

[19] H. Demirtas and D. Hedeker, A practical way for computing approximate lower and upper correlation bounds, *The American Statistician*, **65**(2), (2011), 104-109.

[20] C.D. Vale and V.A. Maurelli, Simulating multivariate nonnormal distributions, *Psychometrika*, **48**(3), (1983), 465–471.

[21] T.C. Headrick and S.S. Sawilowsky, Simulating correlated multivariate non-normal distributions: Extending the Fleishman power method, *Psychometrika*, **64**(1), (1999), 25–35.

[22] T.C. Headrick, A characterization of power method transformations through *L*- moments, *Journal of Probability and Statistics*, **2011**, Article ID 497463, (2011), 22 pages.

[23] F.A. Hodis, T.C. Headrick and Y. Sheng, Power method distributions through conventional moments and *L*-moments, *Applied Mathematical Sciences*, **6**(44), (2012), 2159-2193.

[24] M.D. Pant and T.C. Headrick, A doubling technique for the power method transformations, *Applied Mathematical Sciences*, **6**(130), (2012), 6437-6475.

[25] F.A. Hodis and T.C. Headrick, A system of power method distributions based on the logistic, normal, and uniform distributions, Paper presented at the annual meeting of the Mid-Western Educational Research Association, St. Louis, MO, USA, (2007).

[26] F.A. Hodis, *Simulating univariate and multivariate non-normal distributions based on a system of power method distributions*, Unpublished doctoral dissertation, Southern Illinois University, Carbondale, IL, USA, 2008.

[27] T.C. Headrick and R.K. Kowalchuk, The power method transformation: Its probability density function, distribution function, and its further use for fitting data, *Journal of Statistical Computation and Simulation*, **77**, (2007), 229-245.

[28] S. Morgenthaler and J. W. Tukey, Fitting quantiles: Doubling, HR, HQ, and HHH distributions, *Journal of Computational and Graphical Statistics*, **9**, (2000), 180-195.

[29] J.R.M. Hosking, *L*-moments: Analysis and estimation of distributions using linear combinations of order statistics, *Journal of the Royal Statistical Society, Series B,* **52**(1), (1990), 105–124.

[30] J. R. M. Hosking, Moments or *L*-moments? An example comparing two measures of distributional shape, *The American Statistician*, **46**(3), (1992), 186–189.

[31] J.R.M. Hosking and J.R. Wallis, *Regional Frequency Analysis: An Approach Based on L-Moments*, Cambridge University Press, Cambridge, UK, 1997.

[32] T.C. Headrick and M.D. Pant, Simulating non-normal distributions with specified L-moments and L-correlations, *Statistica Neerlandica,* **66**(4), (2012),422–441.

[33] M. Kendall and A. Stuart, *The Advanced Theory of Statistics*, Macmillan, New York, NY, USA, 4th edition, 1977.

[34] M. D. Pant and T. C. Headrick, A method for simulating Burr Type III and Type XII distributions through *L*-moments and *L*-correlations, *ISRN Applied Mathematics*, vol. 2013, Article ID 191604, (2013), 14 pages.

[35] Microsoft FORTRAN PowerStation Version 4.0. Microsoft Corporation, Redmond, Wash, USA, 1994.

[36] TIBCO Spotfire S+ 8.2.0 for Microsoft Windows. TIBCO Software Inc., Palo Alto, Calif, USA, 2010.

[37] R. Serfling and P. Xiao, A contribution to multivariate *L*-moments: *L*-comoment matrices, *Journal of Multivariate Analysis*, **98**(9), (2007), 1765–1781.

[38] S. Wolfram, *The Mathematica Book*, Wolfram Media, Champaign, Ill, USA, 4th edition, 1999.

[39] Wolfram Mathematica 9.0.0.0 for Microsoft Windows. Wolfram Research Inc., Champaign, Ill, USA, 2012.

[40] G. Marsaglia, Evaluating the normal distribution, *Journal of Statistical Software*, **11**(5), (2004), 1–11.

Appendix

Pearson Correlation Based Procedure for Double-Uniform-PM and Double-Triangular-PM Distributions

Let U_j and T_k be two $Unif(-\sqrt{\pi/2}, \sqrt{\pi/2})$ and $Tri(-\sqrt{2\pi}, \sqrt{2\pi})$ variates of the forms (48) and (49), respectively, where Φ_j and Φ_k are the cdfs associated with standard normal variables Z_j and Z_k. Let $p(U_j)$ and $p(T_k)$ be two random variables of the forms (4) and (5) that are based on U_j and T_k, respectively, and are correlated at the specified Pearson correlation level of ρ_{jk}. Let Z_j and Z_k be correlated at the intermediate correlation level of r_{jk}, with the joint pdf given by (47). The specified Pearson correlation ρ_{jk} between $p(U_j)$ and $p(T_k)$ is given by

$$\rho_{jk} = Cov\left(\left(\frac{p(U_j) - \mu_j}{\sigma_j}\right), \left(\frac{p(T_k) - \mu_k}{\sigma_k}\right)\right)$$

$$= \int_{-\infty}^{+\infty} \int_{-\infty}^{+\infty} \left(\frac{p(U_j) - \mu_j}{\sigma_j}\right)\left(\frac{p(T_k) - \mu_k}{\sigma_k}\right) f_{jk}\, dz_j\, dz_k \qquad \text{(A.1)}$$

where μ_j and μ_k are the means, and σ_j and σ_k are the standard deviations associated with $p(U_j)$ and $p(T_k)$, which can be obtained from equations (7) and (12), and (8) and (13), respectively. Also, note that $p(U_j)$ and $p(T_k)$ can be expressed as piecewise functions in Mathematica [39] source code as in Algorithm 2.

Substituting the value of specified correlation, ρ_{jk}, on the left-hand side and solved values of $C_{\mathcal{L}}$ and $C_{\mathcal{R}}$ together with the values of means and standard deviations and equation (47) on the right-hand side of (A.1) and subsequently integrating (A.1) for $n(n-1)/2$ intermediate correlations r_{jk} so that n specified double-uniform-PM and double-triangular-PM distributions also have a specified correlation structure.